# GULLY HEAD RETREAT OF AWACH-KANO GULLIES, NYANZA PROVINCE, KENYA: FIELD MEASUREMENTS AND PIXEL-BASED UPSLOPE CATCHMENT ASSESSMENT

Yusuke KATSURADA[(1)] Mitsuo HOSHINO[(2)] Koshi YAMAMOTO[(2)]
Hidekazu YOSHIDA[(1)] Kenichiro SUGITANI[(2)]
*Nagoya University Museum*[(1)]
*Graduate School of Environmental Studies, Nagoya University*[(2)]

ABSTRACT Gully erosion is a form of land degradation. Soil loss from croplands and residential areas and damage to human infrastructure caused by gully headcut retreat are particularly serious issues for developing countries in sub-Saharan Africa. We focused on the severe gully headcut retreat that incises agricultural land at the foot of the Kavirondo Rift escarpment in western Kenya. Between 2003 and 2004, measurements of the gully headcut retreat were taken. We investigated the topography, geology, and vegetation cover of the upslope catchment through field studies using remotely sensed imagery, analyzed using pixel-based data management. Analysis showed that factors sensitive to runoff were dominant and different overland flow paths caused different kinds of gully headcut retreat. Our pixel-based catchment assessment is a useful measure in the risk management of gully headcut retreat in this region.

Key Words: Gully erosion; Headcut retreat; Kavirondo Rift; Pixel-based data management; Upslope catchments.

## INTRODUCTION

Most of Kenya is part of the vast area in continental Africa suffering from severe soil degradation. These lands are affected by human-induced water erosion. Runoff and soil loss are particularly strong after disturbances of vegetative cover caused by human actions. Rainfall events tend to be intensive with a high erosive potential (UNEP, 1992). On the Kenyan side of the Lake Victoria basin, which supports one of the densest and poorest populations in the world, discharges from rivers in the extraordinarily pluvial period of 1961 –1964 were 10–20 times higher than their respective 35-year decadal averages, and many of the soil erosion problems started or were accelerated in the early 1960s (Shepherd et al., 2000).

Sediment discharge and erosion amounts on a drainage basin scale have been studied for the sub-Saharan and Sahel regions of the African continent (Grunblatt et al., 1992; Shepherd et al., 2000). Studies of soil erosion on local scales such as the individual gully system have also been conducted in these regions (Oostwoud Wijdenes & Bryan, 2001; Billi & Dramis, 2003; Flügel et

al., 2003). Gully head morphology as a key factor of gully development has also been well studied in Mediterranean environments (Oostwoud Wijdenes et al., 1999; Vandekerckhove et al., 2003). Headward erosion of gullies not only damages local lands but is also an important factor in understanding land degradation problems caused by erosion/sedimentation processes as a whole, and therefore deserves detailed investigation.

Gully erosion is mainly generated and accelerated by overland flow, influenced by runoff occurrence upslope. Basement rocks experience more runoff than unconsolidated sediments when precipitation is minor because of their low permeability, and densely vegetated land surfaces are more resistant to runoff and erosion. From the standpoint of energy, steep slopes generally cause more mass wasting than gentle slopes. Once mass wasting occurs upslope, it may cause a more erosive suspended load. These general facts mean that detecting geological, topographical, and land cover properties can be indicators of different types of erosive potential. However, it is difficult to collect detailed information continuously, especially given the spatial conditions and limited financial resources of sub-Saharan Africa. Our study aims to propose an effective method by which to monitor and predict gully erosion taking into perspective different erosive factors.

We investigated an extremely damaged area called Jimo East in the Nyando District of Nyanza Province, Kenya. Large gullies are deeply incised on Quaternary deposits that lie at the foot of the Kavirondo Rift escarpment, and an untarmacked road has been ruined by these gullies. Erosion at this site is very severe, and the progression of the headward erosion of the gullies threatens the local inhabitants (Fig. 1). The depth of the deepest gully sidewall reaches 14 m. We focused on the headward erosion of the gully heads (gully headcut retreat) and carried out field investigations in the gullied area twice in

**Fig. 1.** Photograph of the gullied area in Jimo East, Nyando District, Nyanza Province, Kenya.

2003 and 2004 to depict the gullying patterns and to measure annual headward erosion.

The gully heads in the study site were divided into two groups according to their spatial pattern. For both groups, the rate of gully head retreat was obtained from field surveys, and the upslope subcatchments for these two gully groups were defined from digital elevation models (DEM) generated from a topographical map. Topographical, geological, and vegetational properties were obtained using image processing and GIS information summarized in a pixel-based database. The area is covered with shrubs on the gently-sloped physiognomy, with basement rocks dominating the upslope catchment. The pixel-based catchment assessment combined with geological observations and remote sensing data can be effectively applied in further investigations of the small-scale gully erosion in this environmental condition with the aim of improving management of erosion risk.

## GEOLOGY AND TOPOGRAPHY OF THE STUDY AREA

The gullied area is located on a dry branch of the river Awach-Kano, a permanent stream of the Nyando River system that flows into Nyakach Bay of Lake Victoria. The study site is located in the Lake Victoria basin in the western plateau of Kenya (Fig. 2). The Lake Victoria basin has been forming within the Precambrian basement under the tensional tectonics of the Kavirondo Rift since the Miocene age (Fig. 3). Thick piles of Quaternary fluviatile and lake deposits infill the basin area and are covered with black-cotton-soil (Saggerson, 1952; Hoshino et al., 2004). The Kavirondo Rift (Shackleton, 1951) branches from the Gregory Rift at the center of the Kenya domal uplift (Baker & Wohlenberg, 1971), with EW and ENE-WSW trend lines towards the Kavirondo Gulf of Lake Victoria (Yairi, 1975). The Nandi and Kendu faults bound the northern and southern edges of the Kavirondo Rift, respectively, and many other faults run parallel to form an east-west fault zone (Saggerson, 1952). Elevation at the bottom of the Kavirondo Rift is approximately 1,200 m above sea level (a.s.l.), and the highest elevations of the Nandi and Kendu escarpments are approximately 1,800 m and 1,700 m a.s.l., respectively. The elevation of the study area, including the upslope catchment, ranges between 1,243 m and 1,656 m a.s.l. (Table 1).

Gullies are incised in the Quaternary deposits. Beds in the Quaternary deposits mainly consist of sand, gravel, and pebbles, and silt beds are found among them. There is calcrete concretion in some beds, which show alternating sand and silt. Although stratigraphic continuity among the beds observed along the gully sidewalls is not confirmed, their bedding planes show a declination of 4 degrees downstream. Figure 4 shows a representative stratigraphy of beds observed at one gully sidewall. The gully channel bifurcates into two branches, and small terraces on top of silty beds were observed in channel beds of both branches. They are discriminative in their shapes—one is more meandering while the other is deeper.

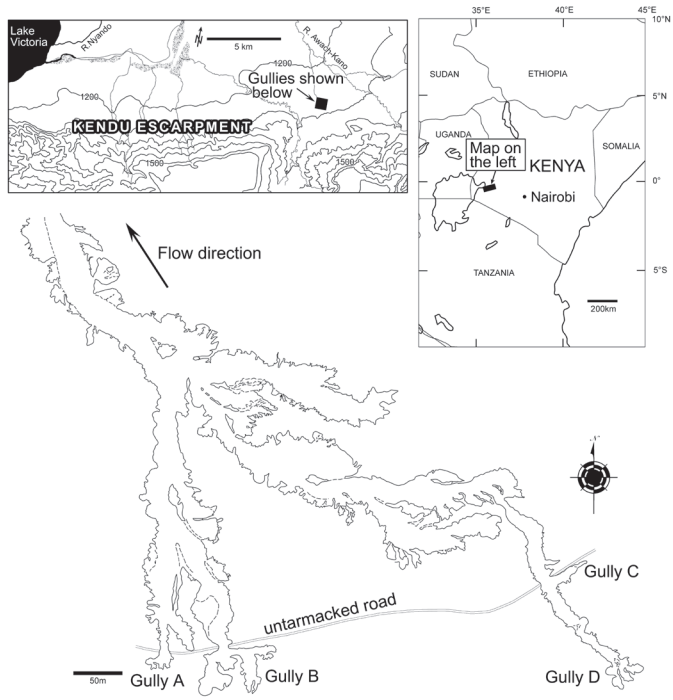


**Fig. 2.** Location of the study area and gullying pattern.
Gullies A and B are located in subcatchment I, and gullies C and D are in subcatchment II. Discontinuous forms such as differences of minor topographic heights inside the gully channels are shown as dotted lines.

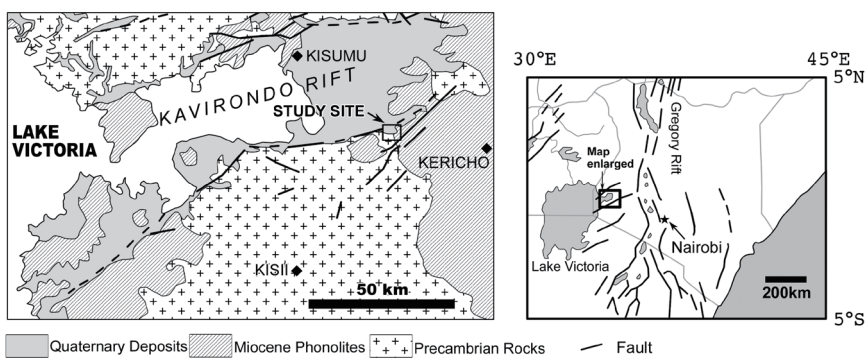


**Fig. 3.** Geological map of the Kavirondo Rift region.

**Table 1.** Topography of the upslope catchment area.

| | elevation (m) | Slope (degree) | Area (ha) |
|---|---|---|---|
| Subcatchment I | 1243 - 1487 | 1.7° – 17.7° | 281.8 |
| Subcatchment II | 1243 - 1656 | 1.7° – 47.3° | 602.7 |

Elevations were calculated from the DEM and slopes were calculated from TIN.

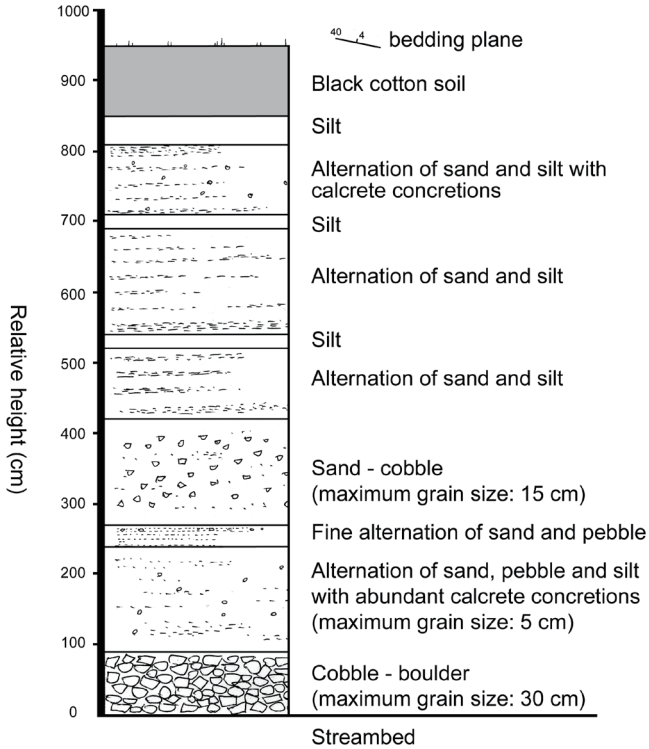


**Fig. 4.** Representative stratigraphy of the gullied area.

Topographical information on the upslope subcatchments was obtained from a 1:50,000-scale topographical map. The topographical map was scanned and digitized. A DEM of sufficiently high resolution is not available for this region, and it is impossible to generate a high-resolution DEM from these topographical maps. Therefore, we generated an original DEM to estimate the upslope catchment areas for the gullies. The method of generating the DEM is described in the next section. The data set of the upslope catchment area is shown in Table 1. The upslope catchments of the gullies have an area of 884.5 ha, and the slope gradient varies between 1.7° and 47.3°.

It rains year-round in this region, but January-February and July-August are comparatively drier periods. Total annual rainfall in this region is between 1,000 and 1,500 mm (Waters & Odero, 1986). Population density of this region is relatively high, and most of the area is settled and cultivated by local people. The average estimated population density in 2000 in the Nyando River basin, including the study area, was 174 (±127) persons per square kilometer (Shepherd et al., 2000).

## METHODOLOGY

The methodology used in this study included field investigation of the gullies, DEM generation of the upslope catchments, gully head retreat estimates, and pixel-based data management of the upslope subcatchments.

### I. Field Investigation

Tape measures, compass, laser rangemeter (Bushnell Yardage Pro 20-1000), and GPS receiver (Garmin e-trex) were used to collect spatial information on gully patterns. Distance and direction between selected points along the gully edges were measured, and the spatial gully patterns were depicted. Positions of these measuring points were calibrated by measuring from the third point, and absolute position was obtained by GPS receiver with a spatial accuracy of ca. 10 m. The whole shape of the gully system in Jimo East was depicted in July and August 2003 (Fig. 2, Hoshino et al., 2004).

The untarmacked road is an important route to a trunk road for inhabitants. It was destroyed in 1997 by gullying at two locations. This road is positioned at a slightly higher elevation (about 1 m) because it is built on a mound; therefore, overland flow should have been intercepted and converged into the gully. This means the erosion processes on either side of the road are different: the upper side is active as a result of overland flow that was concentrated into gully heads. In this research, we focus on the upper, headward erosion in order to ascertain the movement of headcut retreat. Each gully head in these upper gullies was surveyed in detail again in August 2004 to calculate the difference from the survey results of 2003.

### II. DEM Generation

We selected the topographical map "East Africa 1:50,000 (Kenya) Belgut Series Y731 (D.O.S. 423) Sheet 117/3 Edition 5-D.O.S. 1971" as the base-map for DEM generation. Contour lines (20-m interval) of the study area were traced and saved as vector polylines and then rasterized to an image map with 10-m spatial resolution. Two methods were applied to generate the DEM because of their accuracy and reliability. First, the contour line dilation method (Taud et al., 1999) was applied to fill the elevations between traced contour lines, resulting in a DEM with 10-m spatial resolution. Second, the Triangulated Irregular Network (TIN) was produced using the 3D Analyst extension of ArcGIS 9 and was converted to grid data format. These DEMs were used to collect the topographical information of the upslope catchments of the gullies.

### III. Estimate of Gully Head Retreat

Gully heads were named A, B, C and D, as shown in Figure 2. These gully heads were divided into two groups according to position: I (A and B), and II

(C and D). Upslope catchments of both groups were defined from the DEM and were named subcatchments I and II. There were also several subgully heads in each gully head (Fig. 5). Ten subgully heads were detected in gully head A, 27 in B, two in C, and five in D. The linear length of the headward erosion of these subgully heads was determined by measuring the distance between the subgully head points of 2003 and 2004. The gully head areas were defined as areas surrounded by the depicted edges and the line demarcating the gully head, as shown in Figure 5. The downstream ends of the gully heads A and B were defined by the straight lines in Figure 5 since the overland flow can be blocked at the untarmacked road and the headcut retreat occurs selectively on the upslope part of the road. The downstream end of gully head C was defined at the confluence to the main channel. The downstream channel of gully head D is bounded by hedges and compound edges on both banks. Therefore, the downstream end of gully head D was defined at the line shown in Figure 5. Gully head area was determined from the field investigation results for 2003 and 2004 separately.

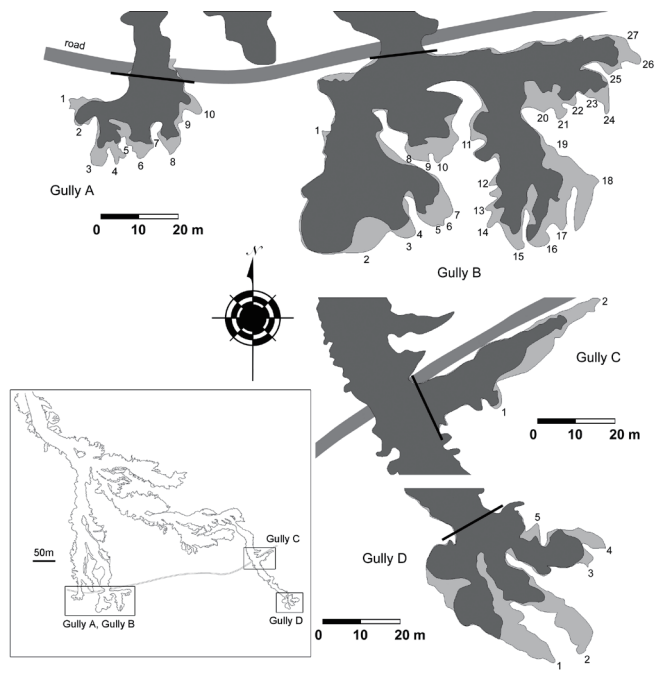


**Fig. 5.** Spatial pattern of the gully head retreat surveyed in 2003 and 2004.
Gullies A and B are located in subcatchment I, and gullies C and D are in subcatchment II. Gullied areas in 2003 and 2004 are shown in darker and lighter tones, respectively. The straight lines indicate the downstream ends of the gully heads.

## IV. Pixel-based Data Management

The vegetative cover of the upslope catchment is an important factor in erosion discussions because runoff rate is affected by vegetation (Morgan, 1986). Remote sensing techniques have recently been applied in soil erosion assessments (Pahari et al., 1996; Singh et al., 2004). A variety of vegetation indices, which have linear relationships with leaf area index (LAI), biomass, leaf water content, chlorophyll, and other biophysical characteristics of vegetation, have been developed (Wiegand et al., 1991; Curran et al., 1992), but the most commonly applied index is the normalized difference vegetation index (NDVI). The NDVI has been widely used in describing relationships between vegetation characteristics such as aboveground biomass, green biomass, and chlorophyll content (Tucker et al., 1985), and it has been applied in African studies—for example, FAO ARTEMIS and NASA PAL archives cover the African continent (FAO/UNEP, 1984; Sannier et al., 1998a,b). However, the spatial resolution of these NDVI archives is not suitable for the gully-head-scale study. Therefore, we selected remotely sensed images of the Advanced Spaceborne Thermal Emission and Reflection Radiometer (ASTER).

ASTER is a research instrument provided by the Ministry of International Trade and Industry (MITI), Japan, and launched on NASA's Earth Observing System Monitoring (EOS-AM1) platform in 1998 (Yamaguchi et al., 1998). The ASTER instrument has three separate optical subsystems: visible and near-infrared (VNIR) radiometer, shortwave-infrared (SWIR) radiometer, and thermal infrared (TIR) radiometer. There are three spectral bands in the VNIR regions with 15-m ground resolution. These three VNIR bands have bandpasses similar to those of the Landsat Thematic Mapper (TM) and the Optical Sensor (OPS) of the Japanese Earth Resources Satellite (JERS-1). These high-resolution data with wide spectral coverage can help to discriminate a variety of surface materials (Yamaguchi et al., 1998).

For the Advanced Very High Resolution Radiometer (AVHRR) band range that overlaps with ASTER VNIR bands, Purevdorj et al. (1998) showed that the NDVI and the transformed soil-adjusted vegetation index (TSAVI) most accurately estimated vegetative cover for grasslands from in situ spectral reflectance data in Japan and Mongolia. Although it is necessary to consider the best vegetation index for African grasslands, we applied the NDVI map generated from ASTER VNIR images to the study site.

NDVI values were calculated from bands 2 and 3 of ASTER VNIR images scanned on 12 December 2003. December is the rainy season in western Kenya. According to the local inhabitants, water erosion occurs only in rainy seasons. The satellite data of the rainy season was therefore selected with the aim of establishing the upslope conditions of this erosion period. Pixels of NDVI values were classified into four classes by clustering with the purpose of simplification of wide-varying NDVI values. These classes are considered representative of vegetation coverage and are numbered 1, 2, 3, and 4 from sparse to dense vegetation. Although no corresponding ground truth data were obtained, class

1 is considered equivalent for bare lands such as gully bottoms, and classes 2, 3, and 4 are for grasslands and croplands such as the ground near the gully heads shown in Figure 6, with shrubs such as *Euphorbia* and *Acacia*, and forests. Catchment outlines were superimposed on the classified NDVI map (vegetation coverage map), and pixels inside the catchment watersheds were carefully clipped out. To relate topographical and geological properties to the vegetation classification, the NDVI pixels were set as a basic grid and slopes and geologies were layered on the pixels.

## RESULTS

### I. Gully Head Retreat

Data of the gully head retreat are shown in Table 2, and the change in spatial pattern is mapped in Figure 5. The darker area in Figure 5 indicates the shapes of the gully heads in 2003, and the lighter area shows the shapes in 2004. Numbers in each gully head indicate subgully heads. The linear lengths of the subgully head positions between 2003 and 2004 were measured, and the average lengths are listed in Table 2.

Gully heads in subcatchment II were extensively eroded, especially for gully head D, as shown in the comparative photographs in Figure 6. The erosion rate of gully head C is lower than that of gully head D because of its position. The length of the gully head retreat differs with the individual subgully heads, but the maximum and average erosion lengths show that the gullies in subcatchment II eroded enormously compared to the gullies in subcatchment I. The depths of the subcatchment I and II gullies are similar: approximately 2 m. Therefore, the ratio of the difference of the spatial patterns can be used to determine the amount of erosion. The ratio of the annual planar change is 1:1.29 for gully heads in subcatchment I : subcatchment II, and the ratio of the linear length of gully head retreat is 1:1.91.

**Table 2.** Gully head retreat during 2003 and 2004.

| | Linear length of retreat | | Projected area of gully heads | | | |
|---|---|---|---|---|---|---|
| | max. $\Delta l$ (m) | ave. $\Delta l$ (m) | $a_{2003}$ ($m^2$) | $a_{2004}$ ($m^2$) | $\Delta a$ ($m^2$) | ratio (%) |
| Gully A | 4.37 | 3.29 | 297.07 | 434.79 | 137.72 | 31.7 |
| Gully B | 9.54 | 4.53 | 2134.29 | 2882.91 | 748.62 | 26.0 |
| Gullies A + B | | | 2431.36 | 3317.70 | 886.34 | 26.7 |
| Gully C | 10.26 | 5.62 | 336.39 | 459.70 | 123.31 | 26.8 |
| Gully D | 17.02 | 9.34 | 600.07 | 969.50 | 369.43 | 38.1 |
| Gullies C + D | | | 936.46 | 1429.20 | 492.74 | 34.5 |

max. $\Delta l$: maximum linear length between subgully heads in 2003 and 2004; ave. $\Delta l$: average linear length between subgully heads in 2003 and 2004; $a_{2003}$: projected area of gully heads in 2003; $a_{2004}$: projected area of gully heads in 2004; $\Delta a$: $a_{2004}$-$a_{2003}$; ratio: $\Delta a/a_{2004}$.

a. Gully head D in 2003

b. Gully head D in 2004

**Fig. 6.** Photographs showing retreat of gully head D in (a) August 2003 and (b) August 2004.

## II. Topography of The Upslope Catchments

The upslope catchments of the two gully head groups were defined from the DEM. The dividing ridges of the upslope catchment were depicted by calculating accumulation of water flow using a contour line dilation-based DEM, except for the flat top of the catchment. This is because the gradient is fairly small near the top of the catchment (Fig. 7a) and it is difficult to determine the watershed. The watershed in the low-gradient part of the catchment was defined using TIN-based DEM.

Slope gradient was calculated for each DEM pixel. However, accuracy is a problem in these calculations, because the TIN-based DEM is inaccurate with its interpolation on ridges, and the contour line dilation-based DEM is interpolated with contours to cause a step-like surface that is parallel to the contour lines because of its algorithm. To avoid these problems, pixels with a 0-degree gradient on slopes for the contour line dilation-based DEM were replaced with

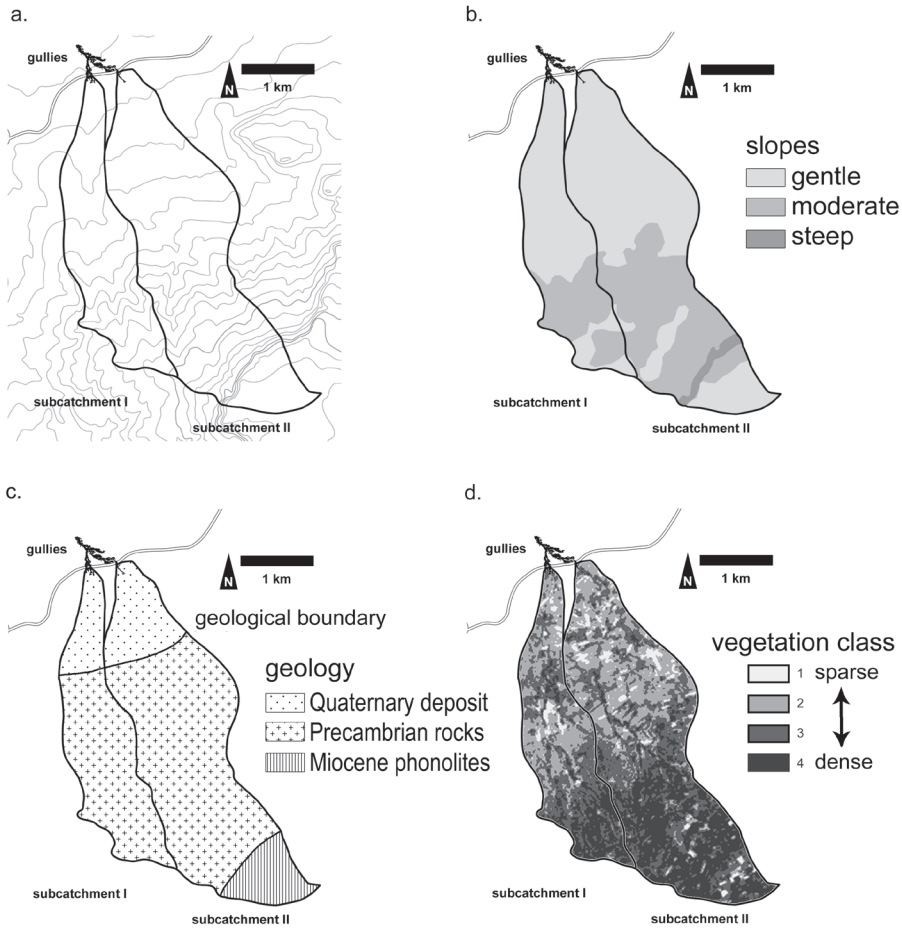


**Fig. 7.** Properties of the upslope catchments: (a) topography (contour line interval is 20 m), (b) slopes (gentle: 0–6°; moderate: 6–30°; steep: 30°–), (c) geology, and (d) vegetation class.

surrounding gradients derived from TIN-based slope surfaces and classified as zones of gentle, moderate, and steep slopes, as shown in Figure 7b. Gentle slopes have a range of approximately 0–6°, and moderate and steep slopes have ranges of approximately 6–30° and >30°, respectively. Areas of these classified slopes (gentle, moderate, and steep) were measured and summarized in Table 3.

III. Land Cover and Geology

NDVI values range between -1 and 1, but the values obtained by NDVI calculation for this catchment from the ASTER VNIR data ranged between -0.07 and 0.83. All pixels were classified into four classes by clustering, as described

**Table 3.** Slopes, geology and vegetation parameters for the two subcatchments.

| | | Subcatchment I | | Subcatchment II | |
|---|---|---|---|---|---|
| | | ha | % | ha | % |
| slope | gentle | 190.4 | 67.6 | 355.1 | 58.9 |
| | moderate | 91.3 | 32.4 | 232.7 | 38.6 |
| | steep | 0 | 0 | 14.9 | 2.5 |
| geology | deposits | 58.2 | 20.7 | 98.3 | 16.3 |
| | basement | 223.5 | 79.3 | 504.4 | 83.7 |
| vegetation | 1 | 10.2 | 3.6 | 26.6 | 4.4 |
| | 2 | 108.6 | 38.5 | 195.1 | 32.4 |
| | 3 | 114.9 | 40.8 | 211.0 | 35.0 |
| | 4 | 48.1 | 17.1 | 170.0 | 28.2 |
| | total | 281.8 | 100 | 602.7 | 100 |

Slope is classified into three classes (gentle: 0–6°; moderate: 6–30°; steep: 30°–), geology is classified into two classes (deposits and basement), and vegetation is classified into four classes (1, 2, 3 and 4) from sparse to dense by clustering NDVI values.

in the previous section (Fig. 7d). The areas of these vegetation cover classes are summarized in Table 3.

It is clear from our field observations that the catchment of the gullies includes three main geological units–Quaternary deposits, basement rocks of Precambrian granites, and Miocene phonolites. From the viewpoint of runoff sensitivity, granites and phonolites were considered to be a single geological unit because these basement rocks have lower permeability than sediments. Quaternary deposits and Precambrian rocks can be divided with the ENE-WSW–trended faults that Shackleton (1951) noted. Remotely sensed data of ASTER SWIR and TIR are useful in defining lithological differences of surface materials by their reflection/emission analyses (Yamaguchi et al., 1998; Rowan and Mars, 2003). However, this method could not be used for this study because of the dense vegetation. From our field observations of the catchment, it was difficult to find the fault outcrops, but we could depict the transition zone of Quaternary deposits and Precambrian granites by referring to the GPS records of our observations. We defined the geological boundary as a center of this transition zone to give the geological parameter to the database pixels (Fig. 7c). The areas of these geological units are shown in Table 3.

## DISCUSSION

The erosion ratio of subcatchments I:II was 1:1.91 for the linear length of the gully head retreat (Table 2). The magnitude relation, i.e., the amount of erosion itself, showed reversal—the amount of gully erosion in subcatchment I was larger than that in subcatchment II by 1.80:1. This is simply because the projected area of gully head B is essentially larger but the relationship of the rate of change (“ratio” in Table 2) is 1:1.29. Thompson (1964) showed that the

gully headcut retreat is proportional to the square root of the catchment area, and the erosion rate estimated in this study exhibits this similarity. The ratio of the square root of the upslope catchment areas is 1:1.46. The numbers of subgully heads in gully heads A and B are greater than those of gully heads C and D (Fig. 5). Headcut retreats of gully heads A and B are smaller but affect a large area, and the retreats of gully heads C and D are larger in a comparatively narrow area. This difference between the two groups of gully heads indicates that there might be controlling factors for both gully channels and upslope catchments.

Field observations indicated geomorphic differences between the gully channels, as previously noted. Taking account of fluvial processes of gully channels, the linear shaped gullies C and D are considered to have been preferentially formed by knickpoint movement accompanied by a lowering process, and this can be a persuasive reason for the rapid headcut retreat; meanwhile, gullies A and B tend to experience sidewall collapse to spread their gully heads horizontally, thereby forming subgully heads. Not only the gully channel morphology, but also overland flow is still an important factor controlling gully headcut retreat. It is necessary to evaluate upslope catchments in cases in which there are differences in any properties between the upslope subcatchments.

To evaluate the upslope catchment of the gullies, topographical and geological properties were layered on the pixel grids of the remotely sensed image. Each pixel is considered a data cell containing parameterized properties. Subcatchments I and II have a total of 16,941 and 37,437 pixels, respectively. Since the topographical property has three parameters (gentle, moderate, and steep slopes), the geological property has two (deposit and basement), and the vegetational property has four (1, 2, 3, and 4), the combined parameters total 24. Table 4 shows the counts of parameterized pixels. Gentle-basement-2 pixels dominate in both subcatchments. Categories with the second and third highest counts are gentle-basement-3 and moderate-basement-3, respectively, for subcatchment I and moderate-basement-4 and moderate-basement-3, respectively, for subcatchment II. These three combinations account for almost the same proportion of between 16 and 20%, and the two subcatchments are characterized by the difference that gentle-basement-3 is larger in subcatchment I and moderate-basement-4 is larger in subcatchment II. There are no pixels of moderate-deposit and steep-deposit in either subcatchment, and steep-basement pixels are found only in subcatchment II.

Some of these parameter combinations can be discussed as runoff-sensitive and mass wasting-sensitive factors according to the properties' nature. Basement rocks with low permeability potentially cause runoff, and steep gradients may cause mass wasting. Therefore, by naming the pixels for "basement" with vegetation class 1 or 2 as runoff-sensitive factors (RSF) and the pixels for "steep" with vegetation class 1 or 2 as mass wasting-sensitive factors (MWSF), the characteristics of a catchment can be profiled. As described above, RSF pixels are dominant for both subcatchments, but basement-3 and basement-4 pixels also have high proportions. Among these pixels, the fraction of "gentle" sloped

**Table 4.** Counts of pixels and percentage of each parameterized pixel for the two subcatchments.

| | | | Subcatchment I | | Subcatchment II | |
|---|---|---|---|---|---|---|
| slope | geology | vegetation | pixels | % | pixels | % |
| gentle | deposits | 1 | 238 | 1.4 | 648 | 1.7 |
| gentle | deposits | 2 | 2227 | 13.1 | 3978 | 10.6 |
| gentle | deposits | 3 | 1057 | 6.2 | 1536 | 4.1 |
| gentle | deposits | 4 | 49 | 0.3 | 100 | 0.3 |
| gentle | basement | 1 | 350 | 2.1 | 897 | 2.4 |
| gentle | basement | 2 | 3329 | 19.7 | 6749 | 18.0 |
| gentle | basement | 3 | 2971 | 17.5 | 5381 | 14.4 |
| gentle | basement | 4 | 1345 | 7.9 | 3278 | 8.8 |
| moderate | deposits | 1 | 0 | 0.0 | 0 | 0.0 |
| moderate | deposits | 2 | 0 | 0.0 | 0 | 0.0 |
| moderate | deposits | 3 | 0 | 0.0 | 0 | 0.0 |
| moderate | deposits | 4 | 0 | 0.0 | 0 | 0.0 |
| moderate | basement | 1 | 22 | 0.1 | 90 | 0.2 |
| moderate | basement | 2 | 973 | 5.7 | 1365 | 3.6 |
| moderate | basement | 3 | 2881 | 17.0 | 6043 | 16.1 |
| moderate | basement | 4 | 1499 | 8.8 | 6550 | 17.5 |
| steep | deposits | 1 | 0 | 0.0 | 0 | 0.0 |
| steep | deposits | 2 | 0 | 0.0 | 0 | 0.0 |
| steep | deposits | 3 | 0 | 0.0 | 0 | 0.0 |
| steep | deposits | 4 | 0 | 0.0 | 0 | 0.0 |
| steep | basement | 1 | 0 | 0.0 | 17 | 0.0 |
| steep | basement | 2 | 0 | 0.0 | 26 | 0.1 |
| steep | basement | 3 | 0 | 0.0 | 146 | 0.4 |
| steep | basement | 4 | 0 | 0.0 | 633 | 1.7 |
| total | | | 16941 | 100.0 | 37437 | 100.0 |

Slope is classified into three classes (gentle: 0–6°; moderate: 6–30°; steep: 30°–), geology is classified into two classes (deposits and basement), and vegetation is classified into four classes (1, 2, 3 and 4) from sparse to dense by clustering NDVI values.

pixels is larger in subcatchment I and the fraction of "moderate" pixels is larger in subcatchment II. Although MWSF appears only in subcatchment II as a fraction of a percent, this is reflected in the physiognomical difference between the subcatchments—subcatchment I is a gentler grassy slope and subcatchment II is a steeper forested hill (Table 2 and 3, Fig. 7).

One hypothesis can now be suggested. The runoff-sensitive condition causes overland flow as a main force of headcut retreat in both subcatchments. Overland flow is dispersed to erode many subgully heads in subcatchment I, and on the other hand, overland flow is concentrated into fewer subgully heads to cause enormous erosion for each subgully head in subcatchment II. Flow paths of the overland flow should be controlled by topographical and geological conditions; furthermore, overland flow with a denser suspended load is more erosive. To verify this hypothesis, more detailed topography, runoff-related param-

eters including permeability, and soil particle detachment rate related to soil properties and vegetation coverage are needed.

The results of this study indicate that the essence of gully headcut retreat may be extracted using the methodology of pixel-based data management. If the spatial distribution of this information were available, pixel-based data management could effectively function to assess gully erosion on a catchment scale. Additionally, taking predictions of the geomorphic processes of channels, ephemeral gullying, and sedimentation downstream into consideration, assessment of not only gully heads in upslope catchments but also the gullying system as a whole, including drainage, may be possible.

ACKNOWLEDGMENTS This study was supported by the Grant-in-Aid for Overseas Scientific Research No. (A)(2) 15253006 from the Japan Society for the Promotion of Science. We are grateful to Mr. Suguru Oho of the Graduate School of Environmental Studies, Nagoya University, whose programs helped our NDVI calculation and DEM modeling using the contour line dilation method.

REFERENCES

Baker, B.H. & J. Wohlenberg 1971. Structure and evolution of the Kenya rift valley. *Nature*, 229: 538–542.

Billi, P. & F. Dramis 2003. Geomorphological investigation on gully erosion in the Rift valley and the northern highlands of Ethiopia. *Catena*, 50: 353–368.

Curran, P.J., J.L. Dungan & H.L. Gholz 1992. Seasonal LAI in slash pine estimated with Landsat TM. *Remote Sensing of Environment*, 39: 3–13.

FAO/UNEP 1984. *Provisional Methodology for Assessment and Mapping of Desertification Report*. Food and Agriculture Organization of the United Nation/United Nation Environment Program, Rome.

Flügel, W.A., M. Märker, S. Moretti, G. Rodolfi & A. Sidorchuk 2003. Integrating geographical information systems, remote sensing, ground truthing and modelling approaches for regional erosion classification of semi-arid catchments in South Africa. *Hydrological Processes*, 17: 929–942.

Grunblatt, J., W.K. Ottichilo, R.K. Sinange, H.A. Mwendwa & J.H. Kinuthia 1992. Kenya: Pilot study for desertification assessment and mapping, Baringo. In (UNEP, ed.) *World Atlas of Desertification*, pp. 54–58. Edward Arnold Publishers, London, U.K.

Hoshino, M., Y. Katsurada, K. Yamamoto, H. Yoshida, M. Kadohira, K. Sugitani, J.M. Nyangaga, N. Opiyo-Akech, E.M. Mathu, W.M. Ngecu, J.I. Kinyamario & E.K. Kangethe 2004. Gully erosion in Western Kenya. *The Journal of the Geological Society of Japan*, 110(2): iii–iv.

Morgan, R.P.C. 1986. *Soil Erosion & Conservation, 2nd ed*. John Wiley and Sons, New York.

Oostwoud Wijdenes, D.J., J. Poesen, L. Vandekerckhove, J. Nachtergaele & J. De Baerdemaeker 1999. Gully head morphology and implications for gully development on abandoned fields in a semi-arid environment, Sierra De Gata, Southeast Spain. *Earth Surface Processes and Landforms*, 24: 585–603.

Oostwoud Wijdenes, D.J. & R. Bryan 2001. Gully-head erosion processes on a semi-arid valley floor in Kenya: A case study into temporal variation and sediment budgeting. *Earth*

*Surface Processes and Landforms*, 26: 911–933.

Pahari, K., S. Murai & J.P. Delsol 1996. *Assessing land degradation using remote sensing and GIS: A case study on soil erosion in Nepal. In: Space Informatics for Grassland Sustainable Development. Proceedings of the First International Seminar on Space Informatics for Sustainable Development: Grassland Monitoring and Management, Ulan Bator, Mongolia*. 20–25 June 1995, 159–166. UNCRD Proceedings Series, no. 10. Nagoya, Japan: United Nations Centre for Regional Development; National Space Development Agency of Japan, 1996.

Purevdorj, T., R. Tateishi, T. Ishiyama & Y. Honda 1998. Relationships between percent vegetation cover and vegetation indices. *International Journal of Remote Sensing*, 19: 3519 –3535.

Rowan, L.C. & J.C. Mars 2003. Lithologic mapping in the Mountain Pass, California area using Advanced Spaceborne Thermal Emission and Reflection Radiometer (ASTER) data. *Remote Sensing of Environment*, 84: 350–366.

Saggerson, E. 1952. Geology of the Kisumu District. *Kenya Geological Survey Report*, 21: 1 –86.

Sannier, C.A.D., J.C. Taylor & K. Campbell 1998a. Compatibility of FAO-ARTEMIS and NASA Pathfinder AVHRR NDVI Data archives for African Continent. *International Journal of Remote Sensing*, 19: 3441–3450.

Sannier, C.A.D., J.C. Taylor, W. Du Plessis & K. Campbell 1998b. Real-time vegetation monitoring with NOAA-AVHRR in Southern Africa for wildlife management and food security assessment. *International Journal of Remote Sensing*, 19: 621–639.

Shackleton, R.M. 1951. Geology of the country between Nanyuki and Maralal. *Kenya Geological Survey Report*, 11: 1–54.

Shepherd, K., M. Walsh, F. Mugo, C. Ong, T. Svan-Hansen, B. Swallow, A. Awiti, M. Hai, D. Nyantika, D. Ombalo, M. Grunder, F. Mbote & D. Mungai 2000. *Improved land management in the Lake Victoria Basin: Linking land and lake, research and extension, catchment and lake basin*. ICRAF, Working paper 2000– 2002.

Singh, D., I. Herlin, J.P. Berroir, E.F. Silva & M.S. Meirelles 2004. An approach to correlate NDVI with soil colour for erosion process using NOAA/AVHRR data. *Advances in Space Research*, 33: 328–332.

Taud, H., J.F. Parrot, R. Alvarez 1999. DEM generation by contour line dilation. *Computers & Geosciences*, 25: 775–783.

Thompson, J.R 1964. Quantitative effect of watershed variables on rate of gully-head advancement. *Transactions of the ASAE*, 7 (1): 54–55.

Tucker, C.J., C.L. Van Praet, M.J. Sharman & G. Van Ittersum 1985. Satellite remote sensing of total herbaceous biomass production in the Senegalese Sahel: 1980–1984. *Remote Sensing of Environment*, 17: 233–249.

UNEP 1992. *World Atlas of Desertification*. Edward Arnold Publishers, London, U.K.

Vandekerckhove, L., J. Poesen & G. Govers 2003. Mid-term gully headcut retreat rates in Southeast Spain determined from aerial photographs and ground measurements. *Catena*, 50: 329–352.

Waters, G. & J. Odero 1986. *Geography of Kenya and the East African Region*. Macmillan Education, London and Basingstoke.

Wiegand, C.L., A.J. Richardson, D.E. Escobar & A.H. Gerbermann 1991. Vegetation indices in crop assessments. *Remote Sensing of Environment*, 35: 105–119.

Yairi, K. 1975. Fault pattern and crustal extension of the Kavirondo Rift Valley in relation to a bifurcating Rift Model. In (K. Suwa, ed.) *1st Preliminary Report of African Studies*, pp. 39–43. Nagoya University, Nagoya.

Yamaguchi, Y., A.B. Kahle, H. Tsu, T. Kawakami, & M. Pniel 1998. Overview of Advanced

Spaceborne Thermal Emission and Reflection Radiometer (ASTER). *IEEE Transaction of Geoscience and Remote Sensing*, 36(4): 1062–1071.

———— Accepted April 18, 2007

Correspondence Author's Name and Address: Yusuke KATSURADA, *Nagoya University Museum, Chikusa, Nagoya 464-8601, JAPAN.*
*E-mail: katsurada@num.nagoya-u.ac.jp*